Identification of the A15 Contours in Multifilamentary Nb_3Sn Wires by Means of a Magnetic Method

Mattia Ortino and Michael Eisterer

***Abstract*—A model for evaluating thecontours of the A15 layer in $\mathrm{Nb_3Sn}$ wires is proposed. These borders, crucial for the correct assessment of the layer current density J_c and the volume layer pinning force $F_p(B)$ are in fact non trivial to assess in some cases from scanning electron microscopy (SEM) polished surface images, eventually leading to non-negligible discrepancies between independent measurements reporting the same $m-H$ or I_c values. A self-reliant method from magnetometry based (Bean) models is proposed, allowing the outer (r_o) and inner (r_i) contours of the A15 phase to be assessed. The magnetic moment of short samples of a prototype powder in tube (PIT) wire with artificial pinning centres (APC) was measured between 6.5 T (H_0) and 6.95 T at 4.2 K in a superconducting quantum interference device (SQUID) magnetometer, allowing the calculation of r_o from the initial slope of dm/dH. Then, the derived function for the remanent magnetic moment $\mathrm{m_{rem}}$ is fit to the experimental data in order to derive r_i, under the condition that the saturation moment exactly matches the experimental value.**

***Index Terms*—A15, artificial pinning, magnetization, $\mathrm{nb_3sn}$.**

I. Introduction

The evaluation of the layer J_c, the critical current flowing through the effective superconducting cross-section of a wire/tape, has always been crucial for the determination of the pinning characteristics of technical superconductors. The relations between the microstructure and the volume pinning force are essential to predict the final superconducting parameters directly from a proper manufacturing control, tuning the heat-treatment and precursor parameters in order to get the desired layer J_c. Nevertheless, the calculation of this current density always passes through an indirect step, whatever the measurement technique (transport current or magnetometry): one has to know the exact cross-section of the superconducting elements, often affected by inhomogeneities throughout the length and the radius of the specimen. The effective single-filament A15 area (cross-section) will be called "A_{eff}" and the number of filaments "N" in the following.

In the specific case of multi-filamentary $\mathrm{Nb_3Sn}$ wires, especially at their prototype stage, the right identification of the effective superconducting phase ("A15 phase") borders turns out to be sometimes ambiguous, possibly leading to non-negligible discrepancies between independent measurements. This is usually due to:

- Morphological differences among the filaments through the cross-section, especially in non-optimized wires (sub-elements bigger than 50 μm);
- Longitudinal inhomogeneities: "sausaging" of the filaments along the wire length can lead to discrepancies when evaluating the cross sections;
- Definition of the "current-carrying element". There is an acknowledged classification of "coarse grain" (CG) and "fine grain" (FG) population in literature, respectively >1 μm and ≤ 150 nm [1], [2], with the first not significantly contributing to transport current. Still, the current density contributions arising from this continuum of sizes is still not fully assessed: how much does a volume of connected 800 nm large grains influence the J_c? Should this "zone" be ascribed to the A15 region?

The last point of this list generates most of the ambiguities when coming to SEM-image evaluation of polished surfaces of $\mathrm{Nb_3Sn}$ wires cross-sections. In PIT wires for example, there is always a transition between CG and FG, stemming from the decomposition of the $Nb_6Sn_5(Cu_x)$ layer preceding the A15 reaction, which leaves traces of a broad distribution of semi-refined grains, as is clear by looking at two adjacent filaments in Fig. 1. In this picture, two adjacent filaments show different A15 geometry and phase/brightness boundaries (brightest part surrounding the dark central leftover Sn-Cu). While the outer contours can be easily evaluated (differences between the Nb-barrier and $\mathrm{Nb_3Sn}$ are evident) the inner ones are more subjective and rely on the experience of the operator.

Therefore, we propose a method to cross-check the r_o and A_{eff}, from magnetometry based models.

II. Experimental

One sample of APC $PIT-Nb_3Sn$ (starting alloy: $\mathrm{Nb-1at.\%Zrtube+Sn/Cu/SnO_2}$ powders, [3]) was used for this study (Fig. 1, 3). It was cut into 3.3–3.7 mm-long straight

Manuscript received November 25, 2020; revised February 9, 2021 and February 25, 2021; accepted February 25, 2021. Date of publication March 4, 2021; date of current version June 11, 2021. This work was supported in part by EASITrain - European Advanced Superconductivity Innovation and Training and in part by the Marie Sklodowska-Curie Action (MSCA) Innovative Training Networks (ITN) and the European Union's H2020 Framework Programme under Grant 764879. *(Corresponding author: Mattia Ortino.)*

The authors are with Atominstitut, TU Wien, Vienna 1020, Austria (e-mail: ortino.mattia@tuwien.ac.at).

Color versions of one or more figures in this article are available at https://doi.org/10.1109/TASC.2021.3063996.

Digital Object Identifier 10.1109/TASC.2021.3063996

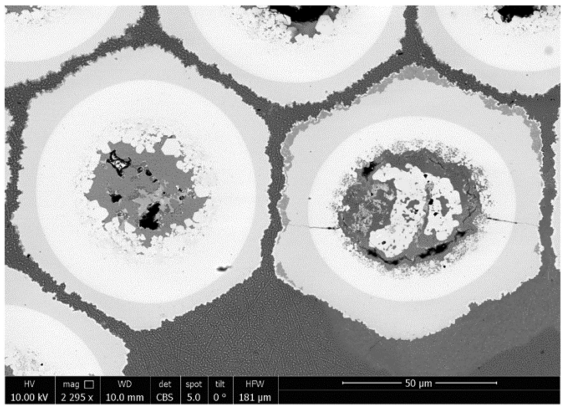

Fig. 1. Two filaments of a 48 sub-elements Nb_3Sn wire. On the right, the CG region is much more evident than on the left, allowing a more direct evaluation of the A15 contours.

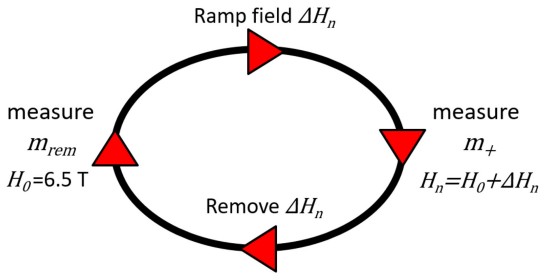

Fig. 2. Measurement sequence: the magnetic moment is measured at H_0, the field is then ramped to H_n and m is measured again, finally back to H_0 where another measurement is performed.

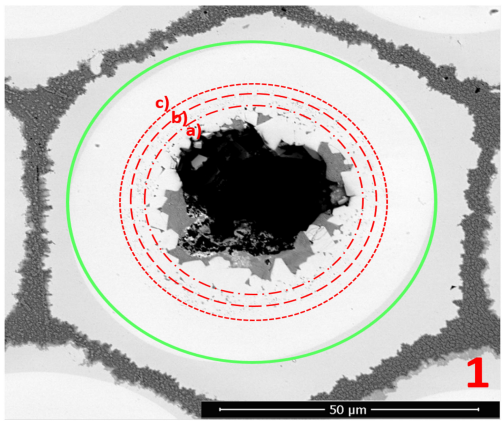

Fig. 3. Three possible choices for r_i, where (a) corresponds to 21.6 μm, (b) to 23.5 μm and (c) to 25.9 μm.

pieces (3 contiguous pieces were cut and tested to aim for consistency) with a low speed diamond saw. Our magnetization measurements were performed in a Quantum Design MPMS XL SQUID magnetometer equipped with a reciprocating sample option (RSO), at 4.2 K with a maximum field of 7 T.

For assessing the filament geometry, the sample was mounted with the wire axis parallel to the applied magnetic field and field-cooled to 4.2 K at 6.5 T. The latter was the base-field H_0 upon which a measurement cycle was performed, chosen because it is above the Nb upper critical field H_{c2}, in the field range of interest and ensuring a negligible variation of J_c. This sequence (field increased - RSO measurement - back to H_0 - RSO measurement) had 30 steps, measuring each time at a higher applied field H_n up to 6.95 T as depicted in Fig. 2.

The field at the n^{nt} step, starting from H_0, was imposed by always adding a field step of 0.01 T as follows

$$H_n = H_0 + \Delta H_n,$$
$$\Delta H_n = n \cdot 0.01\,T \tag{1}$$

The magnetic moment measured at the field H_n is called "m_+," while the one we measure subsequently at H_0 is "m_{rem}," since it is the remaining magnetic moment in the sample.

III. Critical Current Density Evaluation

The standard methods used for characterization of J_c in the state-of-the-art Nb_3Sn samples are:

1) Transport current measurements (V-I): typically performed in cryostats equipped with high-field magnets using the standard 4-points technique. Some facilities allow the whole 0-B_{c2} range to be explored.
2) Magnetic hysteresis loops ($m - H$ cycles): typically performed in the lower-field range, mainly useful when transport measurements are not exploitable. Usually, the pinning force maximum F_{p-max} stays within the applied field range of magnetometry devices (MPMS, PPMS, CCMS).

In the latter case the measured quantity is the "irreversible" magnetic moment m_{irr} (A · m^2), calculated by subtracting the moments measured in increasing and decreasing field of the loop:

$$m_{irr}(B) = \frac{1}{2} \cdot (m_{dec}(B) - m_{inc}(B)), \tag{2}$$

The layer J_c is then derived choosing one of the models in literature [4] as follows:

$$J_c = \frac{3}{4} \cdot \frac{m_{irr}}{NL(r_o^3 - r_i^3)} \tag{3}$$

where L is the length of the sample perpendicular to the applied field and larger than r_o and r_i, the outer and inner radii of the filament-representative hollow cylinder. Indeed, this model assumes all filaments to behave as identical hollow cylinders.

In case 1) instead, the I_c (A) is directly measured, so the expression leading to the layer J_c will be:

$$J_c = \frac{I_c}{A_{eff} \cdot N} \tag{4}$$

where A_{eff} is the effective current carrying A15 area of a filament, usually obtained by image analysis from a representative sample of filaments. It is clear that, for both techniques, the only way to get the layer J_c is to precisely resolve the superconducting phase, with its inner contour being usually the less distinguishable among the two borders.

To better understand the problem, we can extend the assumptions made for magnetometry also to (4) (all filaments behaving as identical hollow cylinders): in this way, since the filaments cross-sections is never a perfect corona, we can intend A_{eff} to

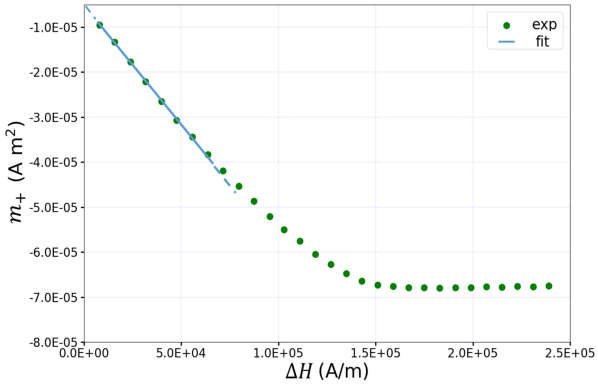

Fig. 4. magnetic moment in increasing field: dm_+/dH_n is evaluated within $7 \cdot 10^4$ A/m (0.08 T) before it saturates.

be the area of an equivalent disc of inner and outer radii r_i and r_o, respectively:

$$A_{eff} = \pi(r_o^2 - r_i^2) \tag{5}$$

This allows us to consistently compare the possible outputs of a wrong evaluation of r_i between the two techniques, as depicted in Fig. 3.

For this filament, the high level of contrast between the phases (and the round-shape of the filament cross-section) allows easily to identify the outer radius r_o, described by the green solid line in Fig. 3. Three radii were then arbitrarily chosen (a, b and c), all of them within the plausible range of choices as they are between the Sn-Cu centre and the outer border of the gloomy CG-region in the SEM-image ($\Delta r_i = 4.3\ \mu$m). The impact on the current evaluation is different for the two experimental methods: for magnetometry (3), choosing r_i to be 21.6 μm (case a) leads to a layer $J_c(r_a = 21.6\ \mu\text{m}) = 0.76 J_c(r_c = 25.9\ \mu\text{m})$. This gap increases when calculating J_c from transport (4): the currents calculated in case a) are 72% of the ones in case c).

IV. Evaluation of Sub Element Geometry

The proposed method stems from Bean's model for the magnetization of hard superconductors [5]. The idea is to measure, safely above the B_{c2} of Nb, the magnetic moment m_+ of the sample until it reaches saturation. Considering the magnetic moment for a hollow cylinder of radii r_o and r_i and length L

$$m = \int_{r_i}^{r_o} JL\pi r^2 dr = \frac{\pi J_c L}{3}(r_o^3 - r_i^3) \tag{6}$$

we first focus on the initial slope of m_+ vs H. Since the measured m refers to the signal coming from all the filaments N in the wire, all the experimental magnetic moments have to be divided by this number.

By looking at Fig. 5 a) we can define the radius where the flux penetration ends

$$r_f = r_o - \frac{\Delta H_n}{J_c} \tag{7}$$

where $\Delta H_n / J_c$ is the slope of the flux front. Combining (7) with (6), together with identifying r_i=r_f (inner radius of the flux front), this yields to

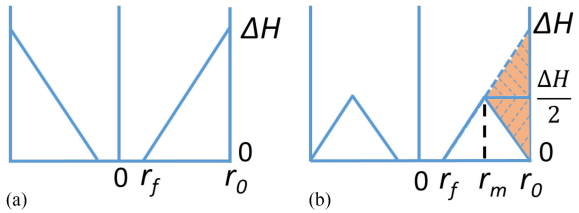

Fig. 5. Bean model for a cylinder in an applied field ΔH_n (a) and the remanent field at 0 T(b).

$$m_+ = -\pi N J_c L \left(r_o^2 \frac{\Delta H_n}{J_c} - r_o \left(\frac{\Delta H_n}{J_c}\right)^2 + \frac{1}{3}\left(\frac{\Delta Hn}{J_c}\right)^3 \right) \tag{8}$$

From (8) we can derive dm/dH by only concentrating on the initial slope of the magnetization

$$\frac{dm_+}{dH_n} = -\pi N r_o^2 L \tag{9}$$

This last formula allows us to directly calculate r_o from our measured m_+, by evaluating dm/dH within $\Delta H_n \leq 7{\cdot}10_4$ A/m (6.5 - 6.58 T). Our calculation gives r_o=34.6 μm, which is as expected really close to what is directly observable from Fig. 3. This derivation is very reliable, since the initial slope of the magnetization curve directly reflects the shielded volume. It is often used to determine or confirm the volume of superconducting samples.

We now focus on m_{rem} to extract r_i [6]. Looking at Fig. 5(b), we can define the remanent magnetic moment which is measured after removing ΔH_n. To get to this quantity we subtract $2m(\Delta H/2)$ (dashed orange areas in Fig. 5(b)) from the magnetic moment m_+ (full triangle area, Fig 5 a). This means:

$$\begin{aligned} m_{rem} &= m_+(\Delta H_n) - 2m_+\left(\frac{\Delta H_n}{2}\right) \\ &= \pi N J_c L \left(\frac{r_o}{2}\left(\frac{\Delta H_n}{J_c}\right)^2 - \frac{1}{4}\left(\frac{\Delta H_n}{J_c}\right)^3 \right) \\ &= \pi N L \left(\frac{r_o}{2J_c}\Delta H_n^2 - \frac{1}{4J_c^2}\Delta H_n^3 \right) \end{aligned} \tag{10}$$

Eq. (10) can be extended to calculate the points above $\sim$ 6.7 T, where m_+ saturates because $r_o - r_i \leq \Delta H / J_c$. By defining ΔH_{sat} as the field at which the saturation occurs, this means:

$$m_{sat} = m_+\left(r_o - r_i = \frac{\Delta H_{sat}}{J_c}\right) \tag{11}$$

where r_i is the inner radius of the sub-element, and

$$m_{rem}(\Delta H_n \geq \Delta H_{sat}) = m_{sat} - 2m_+\left(\frac{\Delta H_n}{2}\right) \tag{12}$$

By sticking to the experimental m_{sat}, we can now calculate J_c as a function of r_i by using (6) and the experimental value of the saturation moment $m_{sat-exp}$. The latter is here the most relevant experimental parameter, as being generally used for evaluating J_c from magnetization measurements.

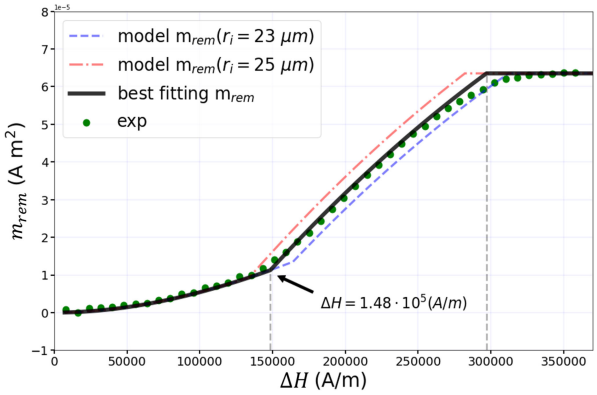

Fig. 6. Experimental and modelled remanent magnetic moment: the green dots are the experimental values; the solid black line represents the best fit to the data, while the red dashed and blue dash-dotted trends are the simulated behaviour for (10) accounting for a slightly longer and shorter r_i, respectively.

This condition for m allows us to calculate J_c as being $3m_{sat-exp}/\pi L(r_o^3 - r_i^3)$.

From $\Delta H_{sat} = J_c(r_o - r_i)$ it is now possible to fit (10) and (12) to the experimental points, thus finding r_i. Fig. 6 shows a consistent match between the calculation and the experimental points by the least squares method, with the vertical lines indicating ΔH_{sat} and $2\Delta H_{sat}$. There is a smooth kink in m_{rem} that corresponds to ΔH_{sat} (also directly observable from m_+, Fig. 4), indicating the flux front to be crossing the border between fine grained and coarse grained area.

The best fit for the function gives $r_i = 24\ \mu$m, which is exactly between the proposed radii b) and c) in Fig. 3. The resulting value for J_c is $1.42 \cdot 10^{10}$ A/m^2. This current should not be confused with the longitudinal current induced when the sample is placed orthogonal to the applied magnetic field. The latter is in fact the usually reported J_c of a sample, as being the useful parameter for technical applications. The difference between these two currents is not necessarily negligible (e.g. cracks, texture [7]): in our case the longitudinal current density was found to be $1.81 \cdot 10^{10}$ A/m^2 [8], thus being $\sim$20% higher than the azimuthal current density at this field and temperature. By using this geometry and (3), the calculated J_c is consistent with literature data [3], [9]. Moreover, these radii are in agreement with independent SEM measurements [10].

Finally, we wish to discuss the stability of the procedure. Comparing the entire theoretical and experimental behaviour of the magnetization process enables an estimation of the reliability of the assumptions in terms of geometry and homogeneity. Fig. 6 demonstrates that the agreement is excellent up to about $1.5\Delta H_{sat}$ but saturation is delayed because of the variation of sub-element geometry. The most massive sub-elements need a higher field to saturate. It is evident that one can derive only representative values for the best description of the hysteretic magnetization, which is exploited by magnetic J_c measurements as well. Therefore, this method represents the most consistent way of choosing the simplified geometry for magnetic J_c measurements.

On the other hand, no clear signs of A15 inhomogeneities can be observed in Fig. 6, which should manifest themselves also by deviations at small fields, if arising from compositional gradients [11]. The best fitting r_i is quite sensitive to the input data, as demonstrated in Fig. 6 by the solid line. A change of r_i by only 1 μm results in a dramatic deterioration of the theoretical description (dashed lines).

V. Conclusion

We proposed a magnetic method for assessing the cross section of the effectively current-carrying elements of a filamentary-structured technical superconductor, when SEM evaluations are not sufficiently reliable. Specifically, this solution is suited for Nb_3Sn multi-filamentary wires, where the contours of the fine-grained A15 region are not clear and applicable to all types of wires whose filaments or sub-elements can be modelled as tubes. The proposed sequence allows to determine the outer and inner radii of the equivalent circular area (cross section) of the current carrying elements, simultaneously. The procedure is quite sensitive to changes in geometry and results in the most consistent values for magnetic J_c measurements. A further advantage is the possibility of deriving the representative A15 geometry for the entire volume of sample not only for one or a few cross sections investigated by SEM. The method may hence be also useful for transport measurements allowing magnetometry to valuably support electron microscopy although the evaluation of resistive measurements does not rely on simplified assumptions about the geometry.

Acknowledgment

The authors gratefully acknowledge Hyper Tech Inc. (Columbus, U.S.) for having provided the sample for this study, and in particular Dr. X. Xu (Fermilab, U.S.) for taking care of the sample heat treatment.

References

[1] C. D. Hawes, "Investigations of the inhomogeneity of a powder-in-tube Nb_3Sn conductor," Univ. Wisconsin–Madison, 2000.
[2] C. Segal, C. Tarantini, P. Lee and D. Larbalestier, "Improvement of small to large grain A15 ratio in Nb_3Sn PIT wires by inverted multistage heat treatments," in *Proc. IOP Conf. Series: Materials Sci. Eng.*, 2017, Art. no. 012019.
[3] X. Xu, J. Rochester, X. Peng, M. Sumption and M. Tomsic, "Ternary Nb_3Sn superconductors with artificial pinning centers and high upper critical fields," *Supercond. Sci. Technol.*, vol. 32, 2019, Art. no. 02LT01.
[4] T. Baumgartner *et al.*, "Evaluation of the critical current density of multifilamentary Nb_3Sn wires from magnetization measurements," *IEEE Trans. Appli. Supercond.*, vol. 22, no. 3, Jun. 2012, Art. no. 6000604.
[5] C. P. Bean, "Magnetization of high-field superconductors," *R*ev. Modern phy., vol. 36, no. 1, pp. 31, 1964
[6] W. R. Rollins, H. Kpfer and W. Gey, "Magnetic field profiles in type'II superconductors with pinning using a new ac technique," *J. Appli. Phys.* vol. 45, no. 12, pp. 5392–5398, 1974.
[7] C. Scheuerlein *et al.*, "Stress distribution and lattice distortions in Nb_3Sn multifilament wires under uniaxial tensile loading at 4.2 K," *Supercond. Sci. Technol.*, vol. 27, no. 4, Mar. 2014, Art. no. 044021.
[8] M. Ortino *et. al.*, "Evolution of the superconducting properties from binary to ternary APC-Nb_3Sn wires," *Supercond. Sci. Technol.* vol. 34, no. 3, Feb. 2021, Art. no. 035028.
[9] X. Xu, M. Sumption, J. Lee, J. Rochester and X. Peng, *J. Alloys Compounds* vol. 845, 2020, Art. no. 156182.
[10] X. Xu, *Private Communication*, vol. 31, no. 5, pp. 1–4, doi: 10.1109/TASC.2021.3063996
[11] T Baumgartner, S. Pfeiffer, J. Bernardi, A. Ballarino and M. Eisterer, "Effects of inhomogeneities on pinning force scaling in Nb_3Sn wires," *Supercond. Sci. Technol.*, vol. 31, no. 8, Jun. 2018, Art. no. 084002.